TU Delft

Delft University of Technology

Experimental study on scour around beveled submerged vanes

Mandal, Anirban; Ahmad, Zulfequar; Mosselman, Erik

DOI
10.1016/j.ijsrc.2025.05.001

Publication date
2025

Document Version
Final published version

Published in
International Journal of Sediment Research

Citation (APA)
Mandal, A., Ahmad, Z., & Mosselman, E. (2025). Experimental study on scour around beveled submerged vanes. *International Journal of Sediment Research*, *40*(5), 791-807. https://doi.org/10.1016/j.ijsrc.2025.05.001

Important note
To cite this publication, please use the final published version (if applicable).
Please check the document version above.

Copyright
Other than for strictly personal use, it is not permitted to download, forward or distribute the text or part of it, without the consent of the author(s) and/or copyright holder(s), unless the work is under an open content license such as Creative Commons.

Takedown policy
Please contact us and provide details if you believe this document breaches copyrights.
We will remove access to the work immediately and investigate your claim.

This work is downloaded from Delft University of Technology.
For technical reasons the number of authors shown on this cover page is limited to a maximum of 10.

International Journal of Sediment Research 40 (2025) 791–807

Contents lists available at ScienceDirect

International Journal of Sediment Research

journal homepage: www.elsevier.com/locate/ijsrc

Original Research

Experimental study on scour around beveled submerged vanes

Anirban Mandal [a, *], Zulfequar Ahmad [a], Erik Mosselman [b]

[a] Department of Civil Engineering, Indian Institute of Technology, Roorkee, India
[b] Faculty of Civil Engineering and Geosciences, University of Technology, Delft, the Netherlands

ARTICLE INFO

Article history:
Received 26 November 2024
Received in revised form
14 April 2025
Accepted 7 May 2025
Available online 12 May 2025

Keywords:
Submerged vane
Bevel angle
Angle of attack
Vane height
Bed morphology
Local scour

ABSTRACT

Submerged vanes are an effective approach to sediment management in river systems. Nowadays, submerged vanes are increasingly utilized in contemporary river engineering due to their convenient and cost-effective installation, which distinguishes them from traditional approaches. However, this structure induces localized scour, which can potentially destabilize and compromise its integrity. The performance and effectiveness of a submerged vane in controlling scour and managing sediment depends on its shape and dimensions. The primary aim of this study is to refine the design of submerged vanes to assess the maximum scour depth in their vicinity and changes in bed morphology downstream of the vane. We carried out 95 experimental runs in clear-water conditions to investigate the influence of vane height, bevel angle, angle of flow attack, and flow regime on the maximum scour depth in the vicinity and downstream of the vane. Results show that the maximum scour depth increases with the increase in the angle of attack, vane height-to-depth ratio, and densimetric Froude number. The depth of scour around the vane and downstream in the channel decreases as the bevel angle increases. We propose empirical equations for calculating the maximum scour depth near the vane and downstream at equilibrium condition. The densimetric Froude number of the flow and the angle of flow attack are found to have the largest influence on maximum scour depth and downstream extension. The findings indicate that the bevel shape is effective method to reduces the maximum scour depth around the vane.
© 2025 International Research and Training Centre on Erosion and Sedimentation. Publishing services by Elsevier B.V. on behalf of KeAi Communications Co. Ltd. This is an open access article under the CC BY-NC-ND license (http://creativecommons.org/licenses/by-nc-nd/4.0/).

1. Introduction

Sediment management in alluvial channels, acting on sediment transport, erosion and deposition, presents a significant challenge for river engineers. Scouring in river bends frequently results in bank destabilization and land loss, whereas sediment deposition on the riverbed often reduces flood conveyance capacity and obstructs channel navigation. Sediment management structures are also essential to minimize sediment entry into the intake, shoaling, and scouring around bridge piers. Although sediment control devices such as groynes and dikes have been utilized, their practical applications have been constrained by structural stability and economic feasibility challenges. Submerged vanes have been developed at the Iowa Institute of Hydraulic Research to address these issues and have been successfully implemented in several countries. Submerged vanes are low-height, elongated structures designed to modify the flow pattern near the riverbed and influence sediment movement in the transverse direction of rivers. These are typically placed at a specific angle to the flow direction within a channel, creating artificial circulations downstream. This occurs due to the pressure difference between the pressure side and the suction side of the vanes (Odgaard & Spoljaric, 1986; Odgaard & Wang, 1991a; Wang & Odgaard, 1993; Klovsky & Kozlov, 2019; Mandal et al., 2024). The induced circulations have been utilized for various purposes, including protecting river banks from erosion (Dey et al., 2017; Odgaard & Mosconi, 1987; Tasar et al., 2023), regulating river migration and reducing shoaling issues (Odgaard & Spoljaric, 1986), managing sediment at lateral diversions (Baltazar et al., 2021; Barkdoll et al., 1999; Gumgum & Cardoso, 2022), and controlling scour at bridge piers and vertical wall abutments (Fathi & Zomorodian, 2018; Hamidi et al., 2024; Vaghefi et al., 2023).

The configuration of a submerged vane has been widely acknowledged as a critical element impacting its enhancement in performance, as highlighted by numerous researchers (Gupta et al.,

* Corresponding author.
E-mail address: anirban_m@ce.iitr.ac.in (A. Mandal).
Peer review under the responsibility of International Research and Training Centre on Erosion and Sedimentation

https://doi.org/10.1016/j.ijsrc.2025.05.001
1001-6279/© 2025 International Research and Training Centre on Erosion and Sedimentation. Publishing services by Elsevier B.V. on behalf of KeAi Communications Co. Ltd. This is an open access article under the CC BY-NC-ND license (http://creativecommons.org/licenses/by-nc-nd/4.0/).

2006; Ouyang, 2009; Ouyang & Lin, 2016). Earlier studies have predominantly focused on rectangular vanes because of their simplicity as per established theories and their ease of fabrication and construction. Consequently, less research has been conducted exploring alternatives to rectangular vanes, including cambered, curved, swept, triangular, and tapered vanes (Barani & Sardo, 2013; Gupta et al., 2006, 2007; Ouyang, 2009; Ouyang & Lin, 2016). Ouyang and Lin (2016) carried out a numerical study of the effectiveness of various vanes. The findings revealed that rectangular and swept vanes increased the bed level near a riverbank by 16% and 17%, respectively, while tapered vanes elevated the bed level by 19%. Gupta et al. (2006) conducted an experimental investigation to determine the performance of double-curved and J-type vanes. Despite equal size and flow parameters, they discovered that the effectiveness of curved and J-type vanes is inferior to rectangular ones. Previous studies show that local scour depth increases with a higher angle of attack (α). Larger α values lead to greater drag force, increased flow resistance, and a heightened risk of significant scour that could dislodge the vane. Therefore, considerable attention is required to minimize local scour around the vane to ensure the feasibility and stability of the submerged vane. With reduced lift at lower angles of attack and a more pronounced drag at higher angles of attack, the optimal range is commonly defined as 15°–30°, as recommended by several researchers (Odgaard & Kennedy, 1983; Odgaard & Spoljaric, 1986). Odgaard and Kennedy (1983) conducted experiments to assess the effectiveness of vanes in reducing near-bank velocity and depth by positioning the vanes at various angles of attack (α). They found that when α exceeds 20°, a scour hole forms at the upstream edge of each vane due to flow separation, and the magnitude of the scour hole diminishes with a decrease in α. Hossain et al. (2004) conducted laboratory tests on scour around bottom vanes. Using experimental data, Hossain et al. (2004) proposed an equation for the maximum scour depth (d_s) (Eq. (1)):

$$d_s = 1.55\left(\frac{HL\sin\alpha}{d}\right)^{0.92} \tag{1}$$

where H denotes the vane height above the undisturbed bed level, L denotes the vane length, and α denotes the angle of attack to flow direction. However, Eq. (1) does not account for flow characteristics and is applicable solely to rectangular vanes. A comprehensive study is necessary to mitigate local scour around vanes by exploring various vane shapes. Barani and Sardo (2013) conducted experiments to compare the effectiveness of flat, angled and curved shapes of rectangular vanes with different arrays and patterns for bank protection. The results indicated that a series of three curved vanes arranged in a zigzag pattern provided superior bank protection compared to other shapes and patterns. Teronpi and Misra (2015) stated that, among rectangular, trapezoidal, and curved vanes, the maximum scour depth occurs specifically with rectangular vanes. Yarahmadi and Bejestan (2016) investigated that triangular vanes provide superior bank protection with spacing at 5 times of the vane's effective length. Azizipour et al. (2020) recommended using slotted vanes along the bank to reduce local scour at the tip of triangular submerged vanes. Their findings indicate that slotted vanes outperform conventional ones in bank erosion protection by decreasing the maximum scour depth. Gabion submerged vanes can also reduce surrounding scour (Sarlak et al., 2023). An experimental study revealed that cutting the leading edge (called bevel shape) of the vanes reduces the local scour around the vanes (Bejestan & Azizi, 2012; Mandal & Ahmad, 2024). Bevel-submerged vanes have been installed at a water intake on the Kosi River, Nepal, to mitigate the entry of sediment as shown in Fig. 1(a). Bevel shapes are known to decrease scour, but no detailed

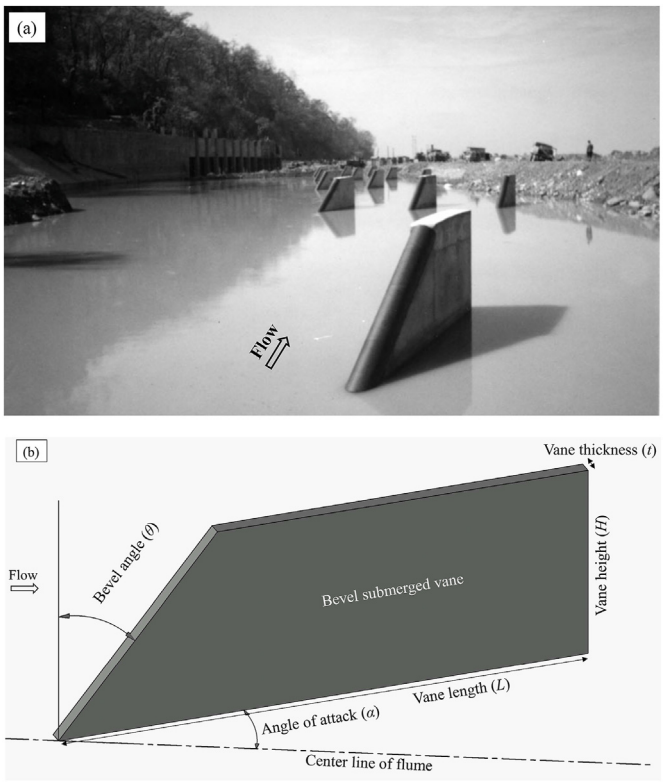

Fig. 1. (a) Bevel submerged vanes being installed at water intake on Kosi River, Nepal (Odgaard, 2009). (b) Definition sketch of bevel submerged vane.

investigations are available to quantify this effect. Also, utilizing a beveled leading edge on submerged vanes can assist in deflecting floating debris that comes into contact with the vane and reducing the construction material. Fig. 1(b) illustrates shape and dimensions of the bevel submerged vane.

In recent times, the use of submerged vanes for various field applications has significantly increased, owing to their ease of installation and cost-effectiveness. One significant drawback of using rectangular submerged vanes is the potential risk of structural failure due to local scour occurring near their tips. It is known that a bevel shape can reduce the local scour, though the extent of the reduction remains uncertain. No calculation methods are currently available to quantify this effect. Hence, additional research is necessary to investigate the optimal design of submerged vanes that can minimize local scour depth around the vane tips and evaluate the impact of vanes on bed morphology. We carried out detailed experimental research on the maximum scour depth and changes in bed morphology due to various dimensions and bevel angles of submerged vane under different flow conditions. We assessed the influence of bevel angle and various other parameters on scour profile, maximum scour depth, and the percentage of scour reduction. Furthermore, we derived an empirical relationship for estimating the maximum scour depth around the vane and in the downstream region from our experimental data.

2. Materials and methodology

2.1. Experimental setup and procedure

A series of experiments was carried out in the Hydraulics Laboratory of Civil Engineering Department, Indian Institute of Technology Roorkee. These runs conducted in a recirculating concrete

flume with a width of 1.0 m, a depth of 0.40 m, and a length of 28 m. The bed slope of the flume is 0.001 (measured by auto level). In the experimental flume, a test section measuring 6 m in length and 0.25 m depth in sediment bed was prepared 10 m from the inlet. The location of the test section was made in such a way that the flow became fully developed before it reaches the test sections followed by Nikora et al. (1998). The sediment bed was prepared with coarse sediment having a median diameter (d_{50}) of 2.36 mm and geometric standard deviation $\left(\sigma_g = \sqrt{D_{84}/D_{16}}\right)$ less than 1.4, indicating a uniform grain size distribution (Marsh et al., 2004). Here D_{84} and D_{16} are grain sizes for which 84% and 16% of the sample are finer than that size by weight, respectively. The relative mass density of sand compared to water was 2.65. Spirit level was used to level the sediment bed of the flume. The sediment bed layer thickness in the test section remained constant at 0.25 m. In each experiment, the submerged vane was positioned on the flume bed's centerline at an angle relative to the incoming flow. Following vane installation, the sediment bed in the flume was re-leveled using a spirit level. The flow rate in the flume was controlled using valves located in the inlet pipes connected to an overhead tank. The discharge (Q) entering the flume was measured using an ultrasonic flowmeter installed on the entrance pipe and with a precision of ±0.0001 m^3/s. A honeycomb masonry wall followed by flow straighteners was installed at 1 m distance from the inlet to ensure a uniform inflow. A tailgate positioned at the downstream end of the flume was used to regulate the uniform flow depth (d) within the test section. At first, to prevent undesired scour caused by sheet flow with insufficient flow depth, the flume was initially filled with water at a low rate by closing the tailgate until the desired flow depth was attained. Subsequently, the discharge in the flume was gradually increased to the desired value, corresponding to the condition of clear-water scour. During the experiment, the flow was increased gradually and the sediment movement was observed visually. Once the sediment starts moving, the discharge and the flow depth were measured and the critical shear stress was computed using $\tau_c = \rho gRS$ and the critical shear velocity of the sediment was computed using $u_{*c} = \sqrt{\tau_c/\rho}$, where ρ is the mass density of flowing fluid, g is the acceleration due to gravity, R is the hydraulic radius, and S is the bed slope. The clear water condition ($u_*/u_{*_c} < 1$, where u_* is the approaching flow shear velocity, and u_{*_c} is the critical shear velocity of the bed sediment) was maintained for all experimental runs, meaning that no sediments travelled from the upstream part of the flume. Flow depths upstream and downstream of the test section were measured using two vernier point gauges accurate to ±0.0001 m. A wooden floater was also used near the inlet of the flume to maintain a smooth water surface. Figure 2(a) shows the schematic plan and section view of the experimental setup. In the experimental flume, the coordinate system was defined with the x-axis representing the streamwise distance along the length of the flume (with $x = 0$ at the middle of the vane), the z-axis representing the lateral distance across the width of the flume (with $z = 0$ at the middle of the vane), and the y-axis representing the depth (or height) from initial bed level in the vertical direction. A schematic diagram illustrating the maximum local scour depth around the vane (d_{sm}) and the extension of the scour hole downstream of the vane (d_{sd}) is presented in Fig. 2(b).

Three-dimensional velocities were recorded using the acoustic doppler velocimetry (ADV) manufactured by Nortek over a duration of 120 s at a sampling frequency of 50 Hz. Signal-to-noise ratio (SNR) of greater than 15 and a minimum signal correlation of greater than 70% were ensured. In post-processing, the experimental data were despiked using a phase-space threshold despiking filter developed as described by Goring and Nikora (2002). The scour profile was measured with the help of a 5 MHz ultrasonic bed

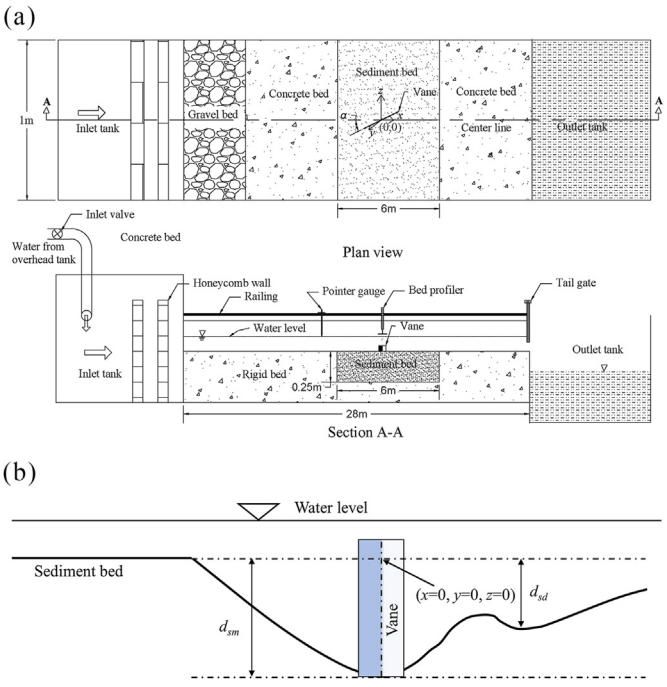

Fig. 2. (a) Diagram illustrating experimental setup. (b) Sketch defining of scour holes at equilibrium scour condition of bed.

profiler. This SeaTek ranging system was composed of 32 transducers and an electronics package. The closest range measurement of this system is 0.035 m; the furthest range is 1 m. In the present study, the sample rate was kept at 1 s, and 100 samples were taken. To check the error in the measurement, a single experiment was repeated multiple times and scour depth was measured. It is found that variations in measured scour depth is negligible. Highly accurate instruments were used for measurement of various parameters. Like, the scour depth was measured using an ultrasonic bed profiler having an optimum accuracy of ±0.0001 m (Best & Ashworth, 1994), and the velocity was measured using ADV having least count of 0.0001 m/s.

2.2. Time to equilibrium

We measured temporal variation of the scour using an ultrasonic bed profiler under three different experimental conditions to determine the time required to reach equilibrium. The temporal

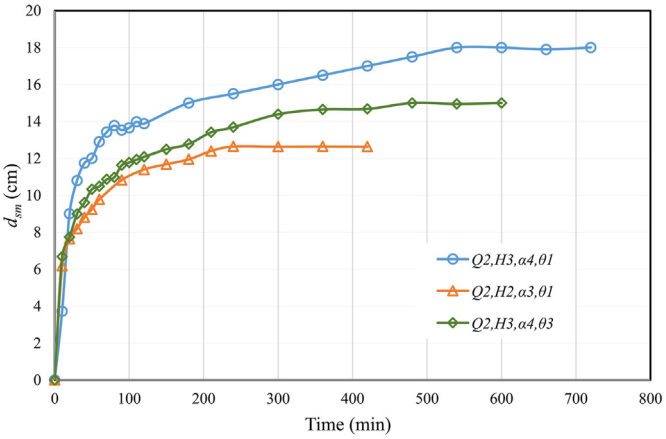

Fig. 3. Temporal variation of scour depth.

variation of the scour depth showed that the maximum scouring occurs in the early 5 h of testing, as shown in Fig. 3. Considering this, the experiments were conducted for 12 h to achieve equilibrium conditions. After that, the pump was stopped, and the water was drained slowly without disturbing the scoured bed by slowly opening the tailgate. A certain scour also occurred due to the displacement of materials from the side slope of the scour hole.

2.3. Range of parameters

We investigated three discharge rates (Q), four angles of attack (α), five different bevel angles (θ), and three vane heights (H), with the specific ranges summarized in Table 1. A total of 95 experimental data for maximum scour depth were collected for various discharge rates, angles of attack, bevel angles, and vane heights. The dimensions of the vanes are determined using the Wang and Odgaard (1993), and Odgaard and Wang (1991a) design criteria: vane height to water depth ratio of H/d = 0.2–0.5, and aspect ratio of H/L = 0.3–0.5.

A table outlining the experimental scheme is included in Appendix 1.1 and Table 5.

3. Dimensional analysis

The maximum scour depth in the local area of the vane and extension of the scour hole downstream of the vane depend on various parameters, namely sediment size (d_{50}), acceleration due to gravity (g), channel width (B), depth of water (d), discharge (Q), average velocity of the flow (V), height of vane (H), length of vane (L), mass density of flowing fluid (ρ), mass density of the sediment (ρ_s), dynamic viscosity of the flowing fluid (μ), bevel angle (θ), and angle of attack (α). Following the method outlined by Ansari and Ahmad (2024), we conducted a dimensional analysis to establish the functional relationship for d_{sm}.

From dimensional analysis, a relation between the previous variables with the maximum scour depth can be developed as Eq. (2):

$$d_{sm} = f(d_{50}, B, g, \mu, \rho, d, Q, H, L, \theta, \alpha) \tag{2}$$

Considering V, ρ, and d as repeating variables and applying the Buckingham (1915), the following non-dimensional Π terms were derived (Eq. (3)):

$$\Pi_1 = \frac{d_{sm}}{d}, \Pi_2 = \frac{d_{50}}{d}, \Pi_3 = \frac{gd}{V^2}, \Pi_4 = \frac{\nu}{Vd}, \Pi_5 = \frac{\rho_s}{\rho}, \Pi_6 = \frac{B}{d},$$

Table 1
Parameter range used for experimental test.

Parameter	Unit	Value	Notation
Discharge (Q)	m^3/s	0.058	$Q1$
		0.082	$Q2$
		0.092	$Q3$
Angle of attack (α)	°	15	$\alpha 1$
		20	$\alpha 2$
		30	$\alpha 3$
		40	$\alpha 4$
Bevel angle (θ)	°	0	$\theta 1$
		30	$\theta 2$
		45	$\theta 3$
		60	$\theta 4$
		70	$\theta 5$
Vane height (H)	m	0.045	$H1$
		0.060	$H2$
		0.075	$H3$

$$\Pi_{76} = \frac{L}{d}, \Pi_8 = \frac{H}{d}, \Pi_9 = \theta, \Pi_{10} = \alpha \tag{3}$$

The functional relationship may be written as (Eq. (4)):

$$\frac{d_{sm}}{d} = f\left(\frac{d_{50}}{d}, \frac{gd}{V^2}, \frac{\nu}{Vd}, \frac{\rho_s}{\rho}, \frac{B}{d}, \frac{L}{d}, \frac{H}{d}, \theta, \alpha\right) \tag{4}$$

We rearrange the non-dimensional Π_2, Π_5, and Π_8 terms as Eq. (5):

$$\Psi_1 = \sqrt{\frac{1}{\Pi_2}\frac{1}{\Pi_3}\frac{1}{\Pi_5}} = \sqrt{\frac{V^2 d}{g d d_{50}\frac{\rho_s}{\rho}}} = \frac{V}{\sqrt{g d_{50}\frac{\rho_s}{\rho}}} = F_D \tag{5}$$

where F_D represents the densiometric Froude number corresponding with different discharges. Since B and L are constant, the effects of Π_6 and Π_7 are negligible. As the flows is turbulent, the kinematic viscosity (ν) has minimal impact on maximum scour depth so that Π_4 can be ignored (Rajaratnam, 1981).

The functional relationship can now be expressed as Eq. (6):

$$\frac{d_{sm}}{d} = f\left[\frac{H}{d}, \theta, \alpha, F_D = \frac{V}{\sqrt{g\left(\frac{\rho_s}{\rho} - 1\right)d_{50}}}\right] \tag{6}$$

Following the same procedure, d_{sd}/d can be expressed as Eq. (7):

$$\frac{d_{sd}}{d} = f\left[\frac{H}{d}, \theta, \alpha, F_D = \frac{V}{\sqrt{g\left(\frac{\rho_s}{\rho} - 1\right)d_{50}}}\right] \tag{7}$$

4. Results and discussion

4.1. Velocity field

At trailing edge, velocity measurements were made at eleven lateral positions across the channel between 0.1 m right and left from the middle of the vane ($z = 0$) with intervals of 0.025 m. At

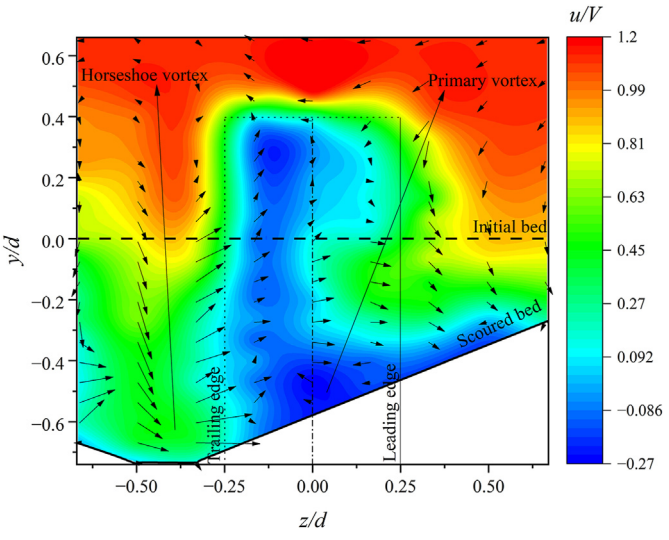

Fig. 4. Normalized contour plot of stream-wise velocity (u/V) background and Normalized vector plot of the velocity field ($\sqrt{(v^2+w^2)}/V$) at trailing edge of the vane.

each lateral position, instantaneous velocities were measured at various depths using Nortek ADV in along the depth. Figure 4 shows the normalized contour profile of stream-wise velocity and normalized vector field in the y–z plane at the trailing edge for $\alpha = 30°$, $H = 0.06$ m, and $\theta = 0°$. A downward flow was observed on the pressure side of the vane, as illustrated in Fig. 4, leading to the generation of a horseshoe vortex. This horseshoe vortex plays a crucial role in generating local scour on the pressure side of the vane. Another vortex was observed at the trailing edge of the vane known as primary vortex, generating a counter velocity field along with a clockwise rotational motion, as can be seen in Fig. 4. The primary vortex altered the velocity distribution, generating a counter-flow region at the trailing edge. The orientation of the vane against the flow generated a pressure difference between its two surfaces, producing an upward flow component on the pressure side and a downward flow component on the suction side. The pressure difference between the pressure and suction side of the vane generated a primary vortex that travelled downstream. This phenomenon is also described in previous literature (Odgaard & Wang, 1991a; Wang & Odgaard, 1993). The horseshoe vortex generated from the leading edge also appeared and vanished quickly, playing a significant role in the local scour on the flow-facing side of the vane, as described by Odgaard and Spoljaric (1989), and Marelius and Sinha (1998).

4.2. Scour analysis

4.2.1. Experimental observation

In none of the experiment sediment movement occurred upstream of the vane, in accordance with the intended clear-water conditions. Figure 5(a) illustrates the initial sediment bed configuration with a rectangular submerged vane before the experimental run, and Fig. 5(b) shows the equilibrium scour bed after 12 h of the experimental run. After the water was drained, two scour holes became visible due to the vane's orientation angle: one formed locally around the vane, while the other extended downstream after the trailing edge of the vane, as shown in Fig. 5(b). Due to the angle of attack along the flow, the horseshoe vortex along the pressure side of the vane becomes significant enough to transport material away from the scour hole effectively. Observations indicate that more significant scour occurred on the pressure side of the vane, whereas some deposition is noted on the suction side at low angles of attack. Eroded sediment particles from the vicinity of the vane primarily begin to accumulate after a certain distance and continue to spread over a longer distance downstream. The vane's angle orientation creates a pressure difference, leading to an upward flow on the higher part of the pressure side and a downward flow on the suction side. This interaction generates a primary vortex that propagates downstream of the vane, eroding material from the right side and depositing it on the left side along the flow, as illustrated in Fig. 5(b). Another observation reveals that changes made to the bed topography gradually diminish as they move downstream. This phenomenon occurred because the strength of the vortex responsible for generating scour weakened as it moved downstream from the trailing edge of the vane.

4.2.2. Transverse scour profiles

The transverse scour bed profiles were measured by ultrasonic bed profiler for $Q = 0.082$ m^3/s at the leading edge and downstream of the vanes. Fig. 6 shows the transverse scour profile along the leading edge for five bevel angles ($\theta = 0°$, 30°, 45°, 60°, and 70°), three vane heights ($H = 0.045$, 0.06, and 0.075 m), and four angles of attack of 15°, 20°, 30°, and 40°. In all graphs, the zero point ($z = 0$) in the transverse direction indicates the center of the vane. As the angle of attack and vane height increased, the scour hole at the leading edge became more pronounced. The leading edge of the rectangular vane creates the strong horseshoe vortex at leading edge, which generates the intense scour on the pressure side and decay quickly. The vertical horseshoe vortex on the pressure side drives particles downward along the vane and upstream along the bed of the scour hole. The horseshoe vortex plays a significant role in generating local scour on the pressure side of the vane, while the primary vortex originating from the trailing edge persists over a longer distance. A similar observation was reported by Marelius and Sinha (1998); Odgaard and Spoljaric (1989); Wang and Odgaard (1993). Cutting the leading edge at various bevel angles with respect to the vertical axis reduced the strength of the horseshoe vortex near the leading edge. The local scour at the leading edge decreased substantially with an increase in bevel angle. as shown in Fig. 6. The observation shows that the bevel shape effectively reduces local scour at higher angles of attack and vane heights compared to the rectangular vane. Fig. 7 shows

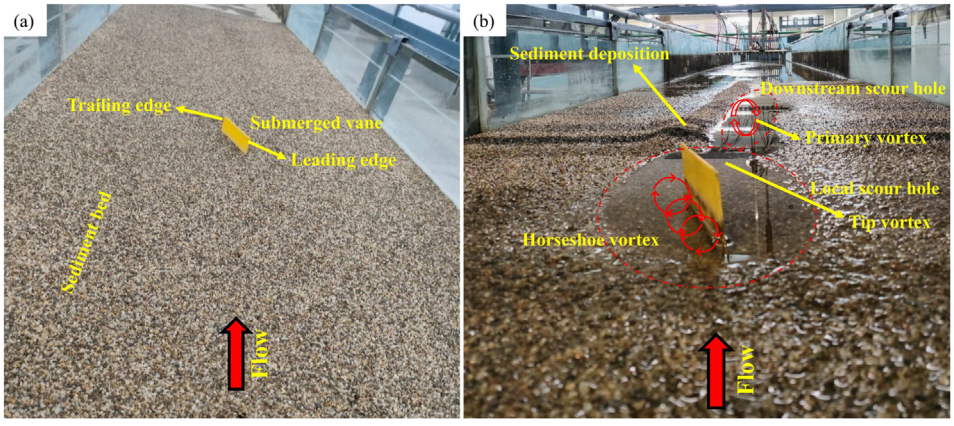

Fig. 5. Photographic images of (a) initial sediment bed condition and (b) equilibrium scour bed condition after the experimental run.

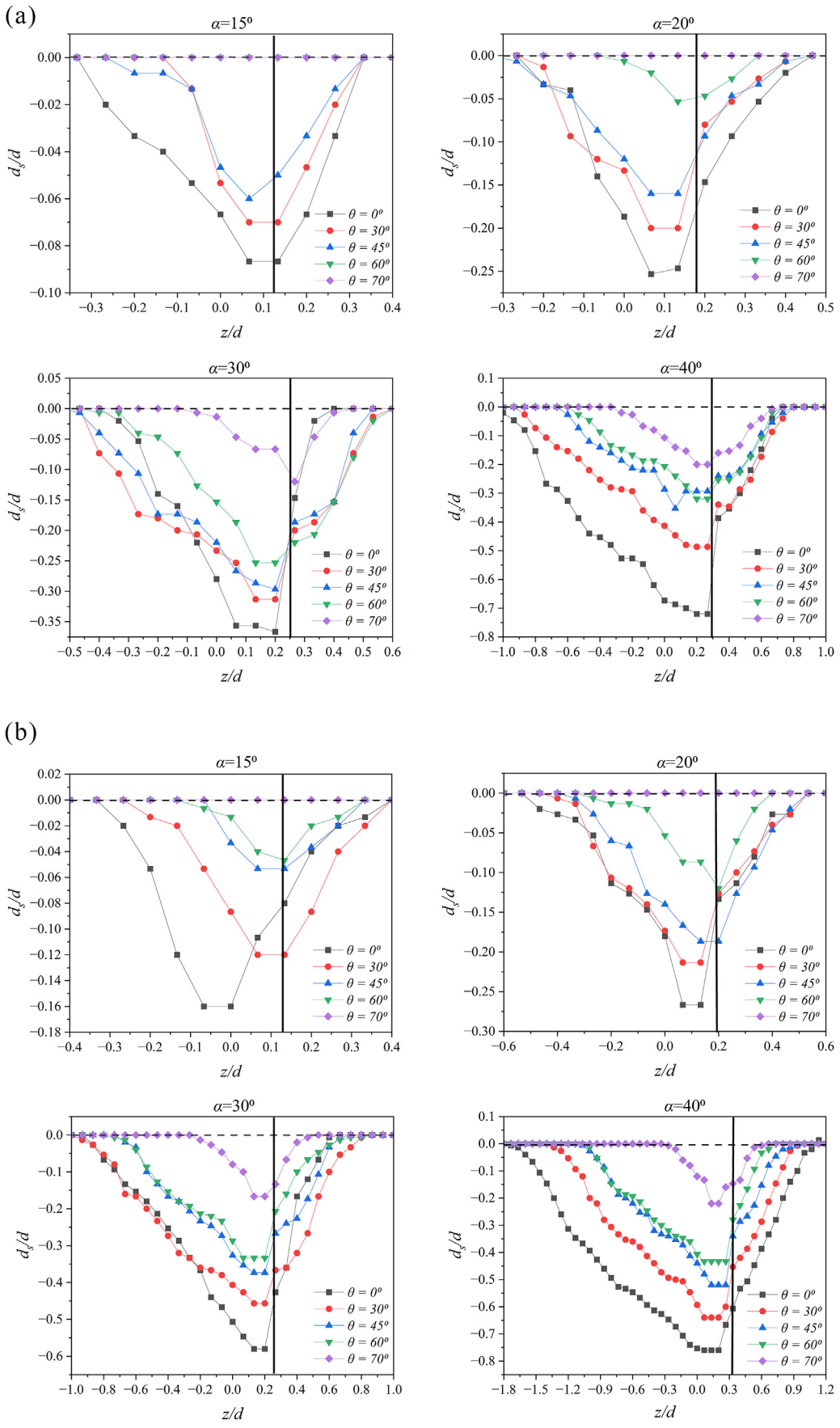

Fig. 6. Transverse scour profiles for $\theta = 0°, 30°, 45°, 60°$, and $70°$ at leading edge, with different angles of attack for (a) $H = 0.045$ m, (b) $H = 0.06$ m, and (c) $H = 0.075$ m. The dashed line and solid line denote the initial bed level and the position of leading edge of the vane, respectively.

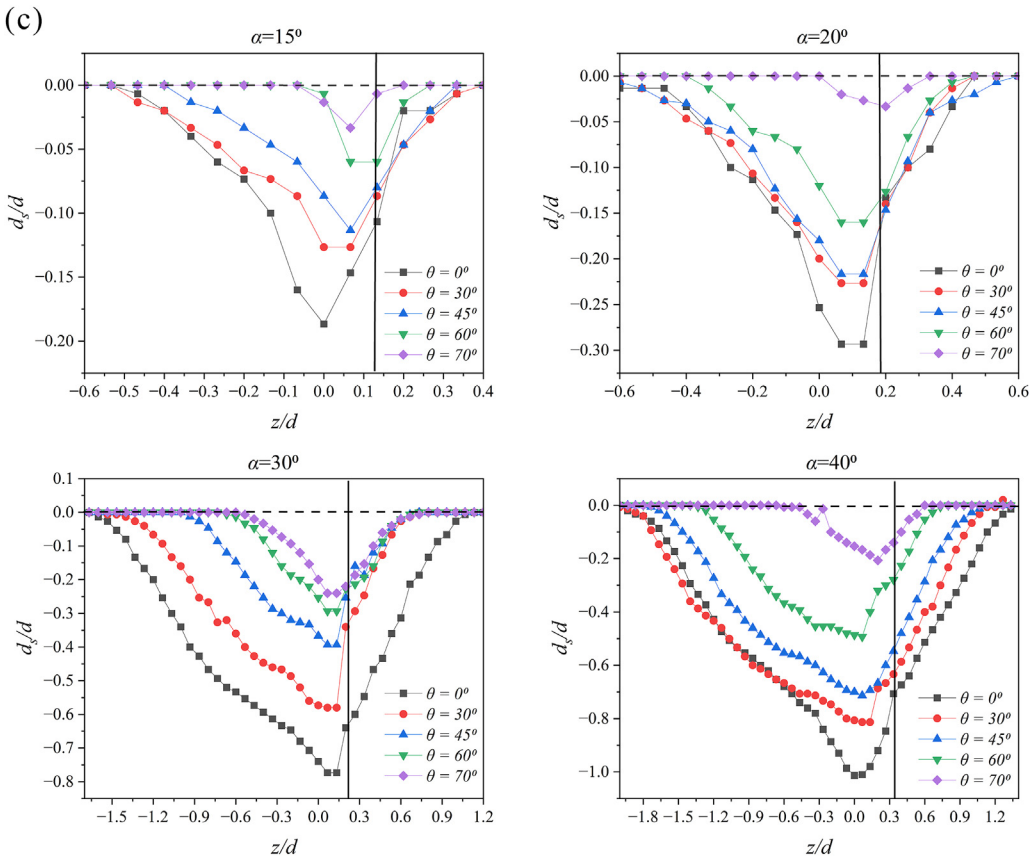

Fig. 6. (*continued*).

the transverse scour profile at a distance downstream corresponding to five bevel angles (0°, 30°, 45°, 60°, and 70°), three vane heights (0.045, 0.06, and 0.075 m), and four angles of attack (15°, 20°, 30°, and 40°). The scour hole downstream of the vane increases with the increasing the angle of attack and the vane height. The primary vortex is responsible for generating scour downstream of the vane, which extends over a considerable distance beyond the trailing edge. The scour and deposition observed downstream of the vane, are shown in Fig. 7. The reduction in local scour became more pronounced compared to the downstream scour as the bevel angle of the vane increased, shown in Figs. 6 and 7. The downstream scour decreased more significantly for bevel vanes at greater vane heights, as the bevel angle results in a greater reduction in the vane's surface area at increased heights, observed in Fig. 7(c).

4.2.3. Scour reduction measurements

Figures 8 and 9 represent the percentage scour reduction due to increasing the bevel angle compare to rectangular vane in different condition of runs. The maximum scour depth around the vane was significantly reduced by cutting the leading edge at various bevel angles. However, the percentage reduction in scour downstream of the vane was less compared to the local scour reduction around the vane as the bevel angles increased, as shown in Figs. 8 and 9. Also, the scour reduction downstream was less compared to the local scour up to the 45° bevel angle. This may be due to the vane's efficiency in generating vorticity not diminishing up to a 45° bevel angle, but instead shifting from the local area to downstream of the vane. Table 2 presents the percentage reduction in the scour depth relative to the maximum scour depth observed for a rectangular vane ($\theta = 0°$) for vane heights of 0.045, 0.06, and 0.075 m and angle of attack of 15°, 20°, 30°, and 40° at both local and downstream scour holes. The efficiency of reducing scour compared to a rectangular vane increased by increasing the bevel angle for all other conditions.

4.2.4. Local scour volume

The scour morphology was measured around the vane by using an ultrasonic bed profiler. Fig. 10 illustrates the variation in scour volume with various bevel angle (θ) for different angles of attack at $H = 0.045$ m and varying vane heights at $\alpha = 20°$. The downward pressure gradient induces a downflow along the front face of the submerged vane, leading to the erosion of a groove in front of and along its pressure side. Consequently, flow separation occurs at the upstream edge of the scour hole formed by the downflow, resulting in the development of a horseshoe vortex. For vanes positioned at greater angles of attack, which strengthen the horseshoe vortex to effectively transport sediment away from the scour hole to downstream. Fig. 10 shows that the volume of scour increases with an increase in both the angle of attack and the vane height, while it decreases with an increasing bevel angle. The rectangular vane generates the strong horseshoe vortex near the vane which create a

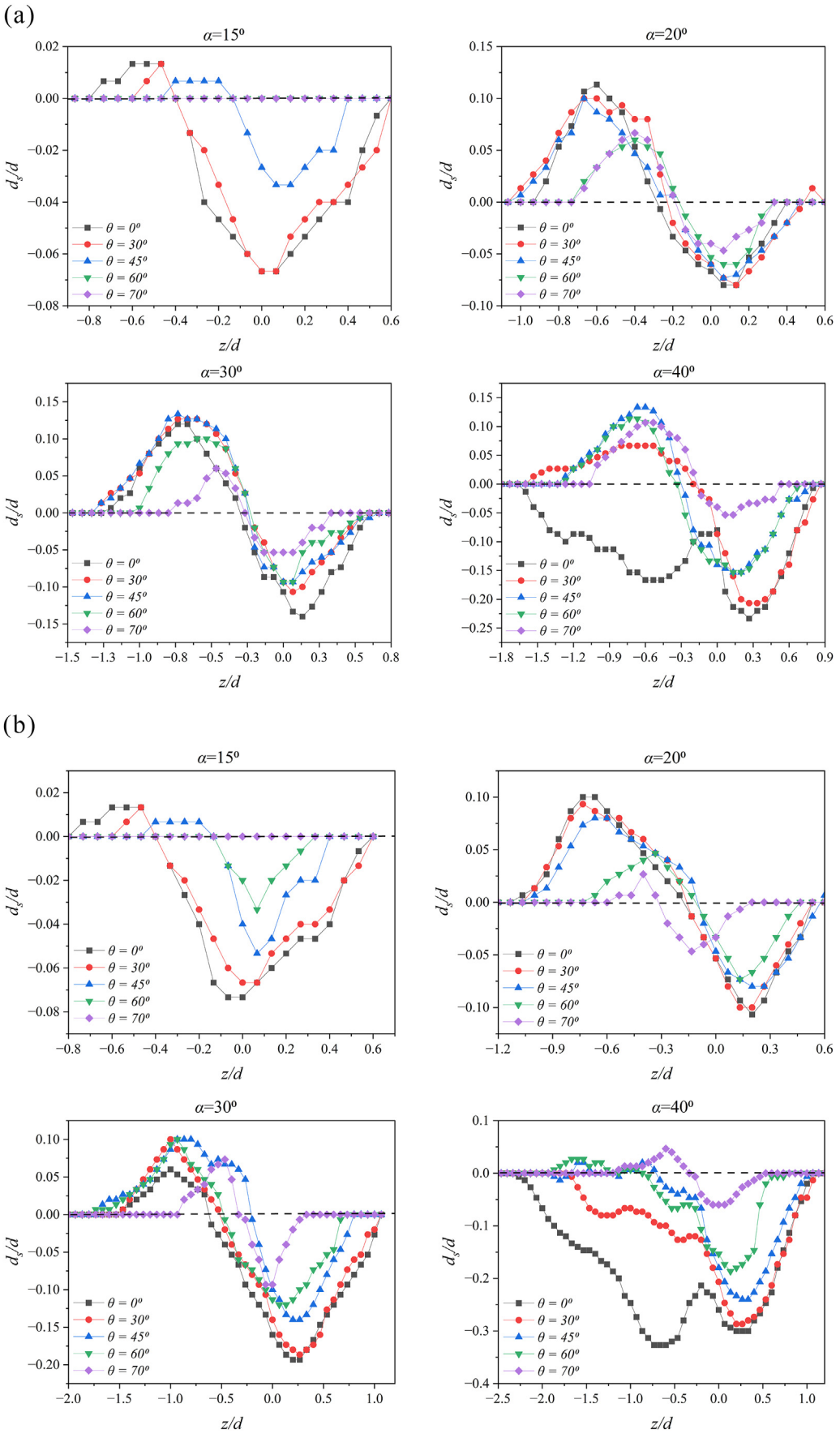

Fig. 7. Transverse scour profiles for $\theta = 0°$, 30°, 45°, 60°, and 70° at downstream, with different angles of attack for (a) $H = 0.045$ m, (b) $H = 0.06$ m, and (c) $H = 0.075$ m. The dashed line denotes the initial bed level.

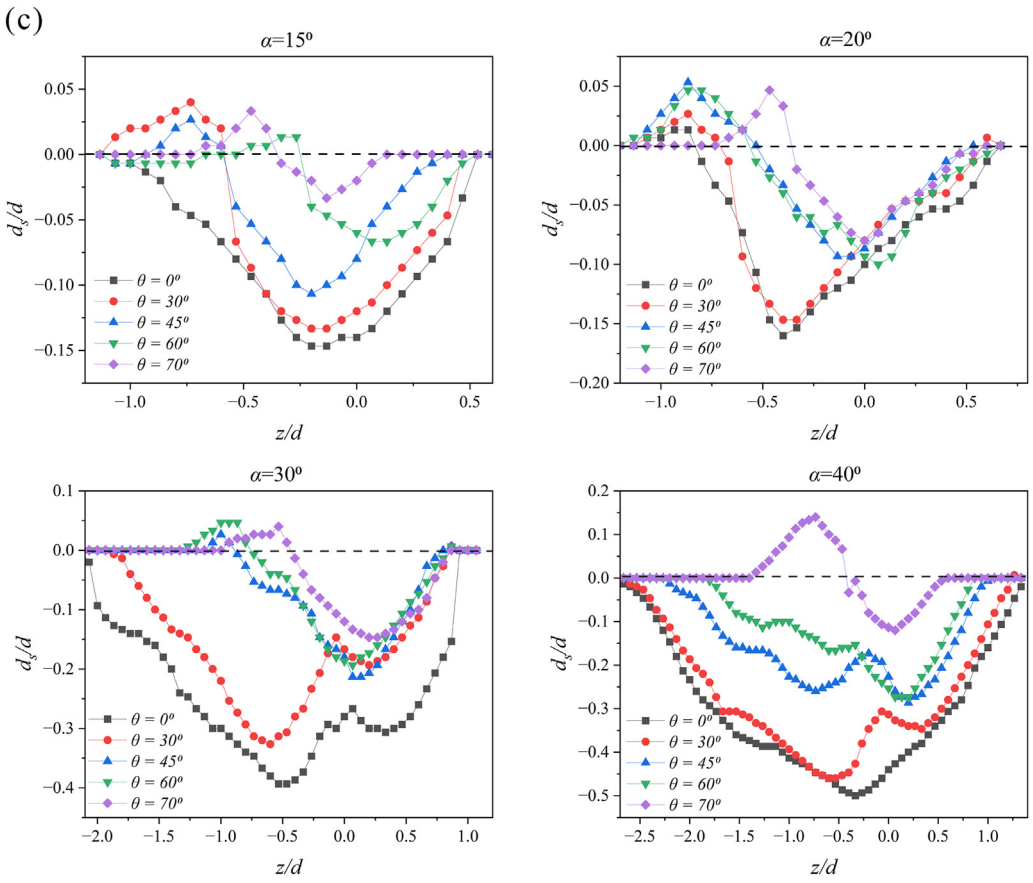

Fig. 7. (*continued*).

significant scour hole around the vane. Cutting the leading edge of the vane significantly weakened this vortex strength, resulting in a substantial reduction in local scour volume compared to a rectangular vane ($\theta = 0°$).

4.3. Influence of various parameters on maximum scour depth

4.3.1. Effect of angle of attack

The variations in maximum scour depth with angle of attack for constant H/d, Q, and θ, is shown in Fig. 11. It is evident that the scour depth was largest at a 40° angle of attack irrespective of the value of H/d, Q, and θ. As seen in Fig. 11, for case $H1/\theta1/Q1$, d_{sm} was 0.01 m for $\alpha = 15°$, increased to 0.031 m for $\alpha = 20°$, 0.065 m for $\alpha = 30°$ and reached a maximum value of 0.088 m for $\alpha = 40°$. A similar trend is observed in all the cases plotted for H, Q, and θ. We infer that the scour depth is maximum when α is maximum for any constant value of H/d, Q, and θ. Increasing the angle of attack caused the vane to generate stronger vortices, which accelerated the development of scour. Odgaard and Spoljaric (1986) conclude that the optimal angle is approximately 15°, as angles exceeding this value result in significant flow separation and excessive local scour. The intensity of the primary vortex increases non-linearly as α increases.

4.3.2. Effect of H/L ratio

Figure 12 illustrates the effects of H/L ratio on the maximum scour depth for constant Q, α, and θ. As seen in Fig. 12, for case $\alpha1/\theta1/Q2$, d_{sm} is 0.019 m for $H/L = 0.3$, and increased to 0.034 and 0.045 m for $H/L = 0.4$ and 0.5, respectively. A similar trend is observed in all the cases plotted for α, Q and θ. We conclude that the scour depth reaches its maximum when the H/L ratio is at its maximum for any constant value of α, Q, and θ. As the ratio of H/L increases, the lift coefficient also rises, likely because the suppression of the tip vortex by the free surface enhances the pressure difference between the vane surfaces. The pressure difference generates a stronger primary vortex, which leads to the formation of a scour hole. Odgaard and Spoljaric (1986) recommend that the H/L ratio ranges from 0.1 to 0.5 for all scour condition flow stages. The present study uses ranges of H/L between 0.3 and 0.5.

4.3.3. Effect of bevel angle

The effects of the bevel angle on d_{sm} for constant H, Q, and α are shown in Fig. 13. The rectangular vane created maximum scour around the vane for any value of H, Q, and α. In the case of $H3/\alpha4/Q2$, d_{sm} is 0.195 cm for $\theta = 0°$, and decreased to 0.165, 0.14, 0.115, and 0.063 cm for $\theta = 30°$, 40°, 60°, and 70°, respectively. A similar trend is observed in all the cases plotted for H, Q, and α. The bevel submerged vane drastically decreased the local scour. The vane's leading edge is the main factor responsible for the formation of the horseshoe vortex, which generates an intense scour depth near the

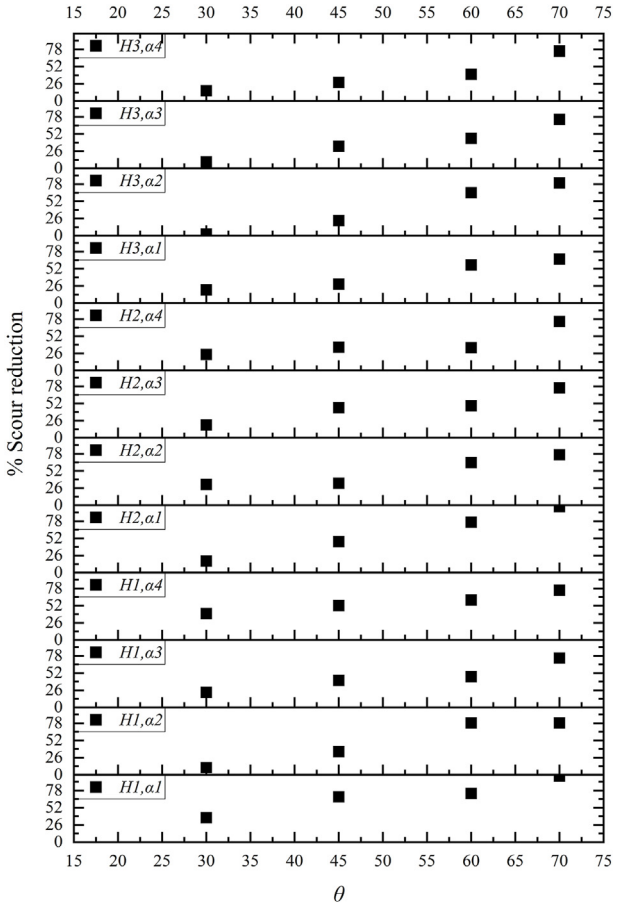

Fig. 8. Efficiency of bevel angle in reducing the % scouring near the vane corresponding to three vane heights (0.045, 0.06, and 0.075 m), and four angles of attack (15°, 20°, 30°, and 40°).

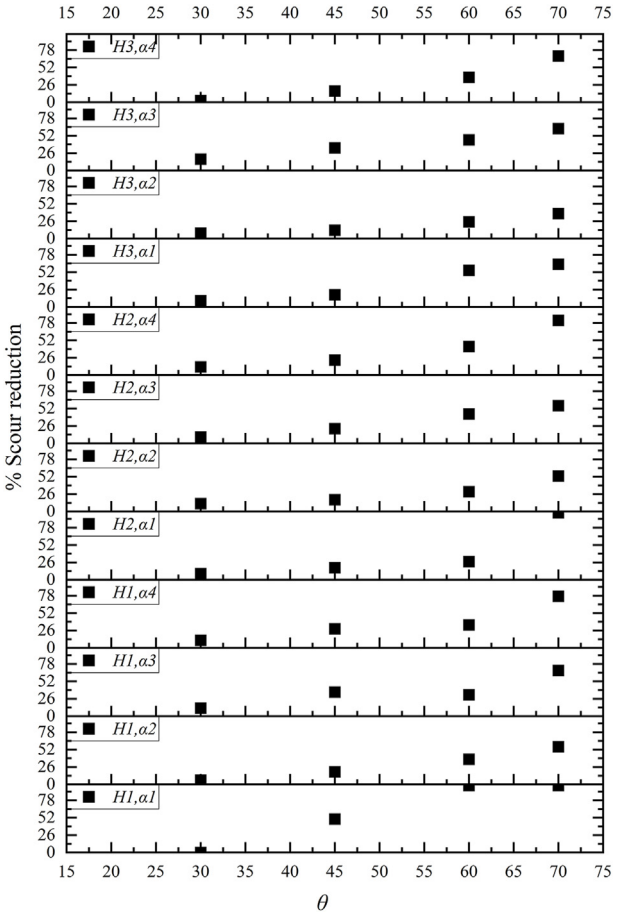

Fig. 9. Efficiency of bevel angle in reducing the% scouring at downstream corresponding to three vane heights (0.045, 0.06, and 0.075 m), and four angles of attack (15°, 20°, 30°, and 40°).

tip and dissipates after a certain distance. Thus, cutting the leading edge (known as bevel vane) minimized the impact of the horseshoe vortex and reduced the maximum scour around the vane.

4.3.4. *Effect of discharge*

The effects of discharge on d_{sm} for constant α, H, and θ are shown in Fig. 14. The maximum discharge generated the maximum scour around the vane. As seen in Fig. 14, for case $H1/\alpha2/\theta1$, d_{sm} is 0.031 m for $Q = 0.058$ m^3/s, and increased to 0.037 m for $Q = 0.082$ m^3/s and 0.042 m for $Q = 0.092$ m^3/s. A similar trend is observed in all the conditions plotted for H, θ, and α. Discharge is the most critical factor in increasing vortex flow around the vane, leading to greater scour in the local area surrounding the vane.

4.4. *Proposed equations for d_{sm} and d_{sd}*

The effects of the individual parameters on d_{sm}/d and d_{sd}/d were examined using graphical analysis. Figs. 15(a)–15(d) demonstrates the effects of H/d, α, θ, and F_D on d_{sm}/d. As evident from Fig. 15, the trend line shows that d_{sm}/d increased with an increase in the H/d, F_D, and α. However, d_{sm}/d decreased with an increase in θ. A similar pattern in the downstream scour hole (d_{sd}) is observed in Figs. 16(a)–16(d). Due to increasing the angle of attack, the vane produced strong vortices in the flow field, leading to an acceleration of scour development. The trend line for local scour depth influenced by various parameters is steeper compared to that of downstream scour depth. Therefore, the local scour around the vane is influenced more significantly by H/d, α, θ, and F_D than the downstream scour.

We derived equations for d_{sm} and d_{sd} from the experimental data in this study and using least-squares curve fitting methods. A randomly selected 80% of the datasets was utilized to develop the equations, while the remaining 20% was employed to validate them. The proposed equation for the maximum scour depth around the submerged vane is as Eq. (8):

$$\frac{d_{sm}}{d} = 1.13\left(\frac{H}{d}\right)^{1.49}(\sin\alpha)^{1.86}(\cos\theta)^{0.99}{F_D}^2 \tag{8}$$

The coefficient of correlation (R^2) for Eq. (8) was determined to assess the linear relationship between the observed and predicted values, resulting in a value of 0.933, which demonstrates a strong agreement between the observed and computed results. The mean absolute percentage error (MAPE) and the root mean square error (RMSE) were calculated to evaluate the model's predictive performance. The values of MAPE and RMSE were 22.3% and 0.09, respectively, which represents the good fit for the prediction. Fig. 17(a) illustrating least-squares method substrates that the

Table 2
Summary of d_{sm} and d_{sd} for bevel angles ($\theta = 0°$, 30°, 45°, 60°, and 70°) with different vane heights ($H = 0.045$, 0.06, and 0.075 cm) and angle of attacks ($\alpha = 15°$, 20°, 30°, and 40°).

α (°)	Scour	θ (°)	$H = 0.045$ m		$H = 0.06$ m		$H = 0.075$ m	
			Scour depth (10^{-2} m)	% reduction	Scour depth (10^{-2} m)	% reduction	Scour depth (10^{-2} m)	% reduction
15	d_{sm}	0	1.9	–	3.4	–	4.5	–
		30	1.2	36.84	2.8	17.65	3.6	20
		45	0.6	68.42	1.8	47.06	3.2	28.89
		60	0.5	73.68	0.8	76.47	1.9	57.78
		70	0	100.00	0	100.00	1.5	66.67
	d_{sd}	0	1.0	–	1.1	–	2.2	–
		30	1.0	0	1.0	9.09	2.0	9.09
		45	0.5	50	0.9	18.18	1.8	18.18
		60	0	100	0.8	27.27	1.0	54.55
		70	0	100	0	100.00	0.5	63.64
20	d_{sm}	0	3.7	–	5.1	–	7.4	–
		30	3.3	10.81	3.5	31.37	7.2	2.70
		45	2.4	35.14	3.4	33.33	5.7	22.97
		60	0.8	78.38	1.8	64.71	2.6	64.86
		70	0.8	78.38	1.2	76.47	1.5	79.73
	d_{sd}	0	1.9	–	1.7	–	2.4	–
		30	1.5	6.25	1.5	11.76	2.2	8.33
		45	1.3	18.75	1.4	17.65	2.1	12.5
		60	1.0	37.50	1.2	29.41	1.8	25.0
		70	0.7	56.25	0.8	52.94	1.5	37.5
30	d_{sm}	0	7.1	–	10.3	–	14.3	–
		30	5.5	22.54	8.3	19.42	12.9	9.79
		45	4.2	40.85	5.6	45.63	9.5	33.57
		60	3.8	46.48	5.3	48.54	7.8	45.45
		70	1.8	74.65	2.5	75.73	3.7	74.13
	d_{sd}	0	2.5	–	3.2	–	5.9	–
		30	1.8	12	2.9	9.38	4.9	16.95
		45	1.6	36	2.5	21.88	3.9	33.9
		60	1.7	32	1.8	43.75	3.2	45.7
		70	0.8	68	1.4	56.25	2.2	62.7
40	d_{sm}	0	12.1	–	12.7	–	19.5	–
		30	7.3	39.67	9.6	24.41	16.5	15.38
		45	5.8	52.07	8.2	35.43	14.0	28.21
		60	4.8	60.33	8.3	34.65	11.6	40.51
		70	3.0	75.21	3.3	74.02	4.8	75.38
	d_{sd}	0	3.5	–	4.9	–	7.8	–
		30	3.1	11.43	4.3	12.24	7.6	2.56
		45	2.5	28.57	3.8	22.45	6.5	16.67
		60	2.3	34.29	2.8	42.86	4.9	37.18
		70	0.8	77.14	0.9	81.63	2.4	69.20

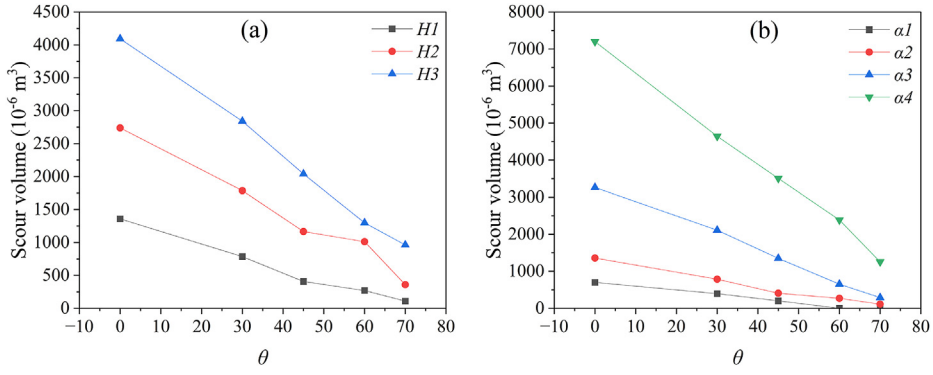

Fig. 10. Variation of local scour volume with various bevel angle (θ) for various (a) vane height (H) and (b) angle of attack (α).

scour depth calculated using Eq. (8) falls within ±25% of the observed values. Equation (8) is applicable for the ranges of $0.04 \le d_{sm}/d \le 1.4$, $0.3 \le H/d \le 0.5$, $15° \le \alpha \le 40°$, $2.66 \le F_D \le 3.22$, and $0° \le \theta \le 70°$.

For the maximum scour depth downstream of the vane, again 80% of the datasets was chosen randomly for training, whereas 20% was used for validation. The resulting equation is Eq. (9):

$$\frac{d_{sd}}{d} = 1.04\left(\frac{H}{d}\right)^{1.57}(\sin\alpha)^{1.66}(\cos\theta)^{0.84}F_D^{1.06} \quad (9)$$

R^2 for Eq. (9) is 0.93, which represent good correlation between the observed and computed results. The values of MAPE and RMSE were 18.1% and 0.035, respectively, which represents the good fit

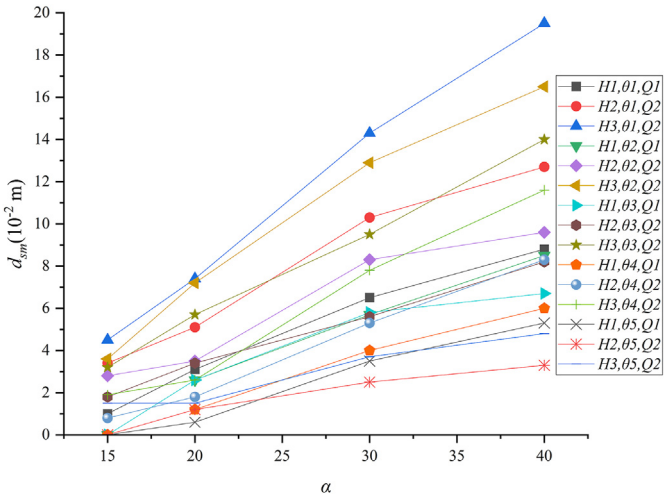

Fig. 11. Variation of maximum scour depth with angle of attack (α).

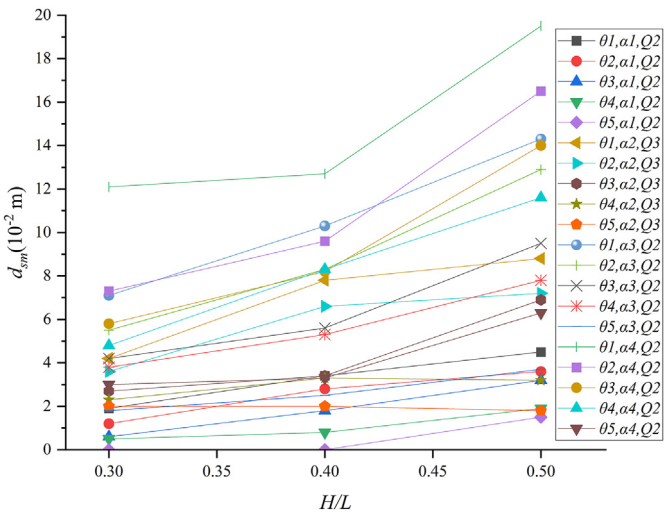

Fig. 12. Variation of maximum scour depth with H/L.

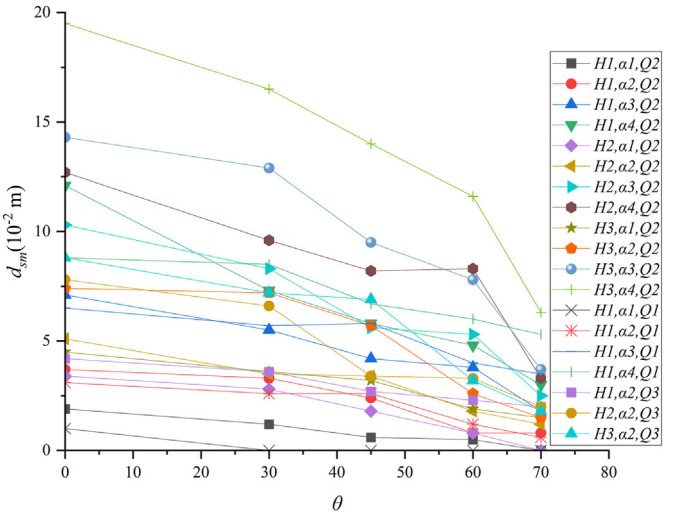

Fig. 13. Variation of maximum scour depth with bevel angle (θ).

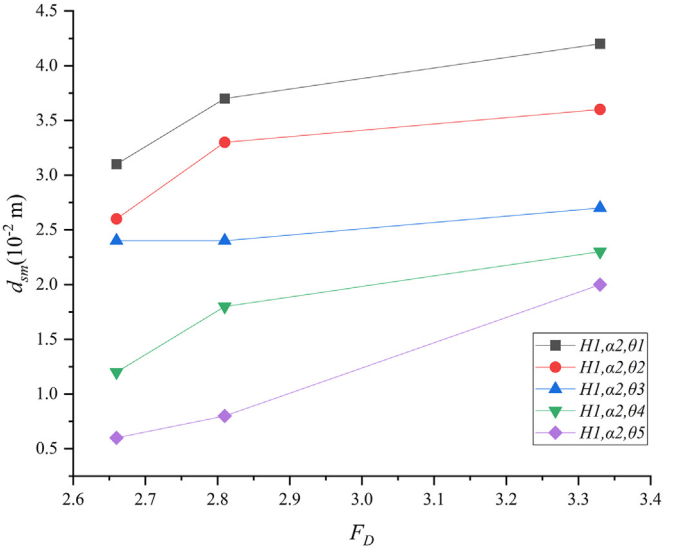

Fig. 14. Relationship between the maximum scour depth and F_D.

for the prediction. Fig. 17(b) illustrates that the scour depth calculated using Eq. (9) falls within ±25% of the observed values. Equation (9) is valid for the ranges of $0.02 \le d_{sm}/d \le 0.51$, $0.3 \le H/d \le 0.5$, $15° \le \alpha \le 40°$, $2.66 \le F_D \le 3.22$, and $0° \le \theta \le 70°$. Equations (8) and (9) were validated for the clear-water condition (meaning that no sediment movement occurred from upstream of the vane) and cohesionless sediment.

We compared the maximum scour depths calculated using Eq. (8) and Eq. (1) with observed values in Fig. 18. The results indicate that the equation proposed by Hossain et al. (2004) underestimates compared to the present Eq. (8). In contrast, the proposed equation (Eq. (8)) predicts values within a ±25 % margin of error. Equation (8) incorporates flow conditions, an aspect not included in the equation proposed by Hossain et al. (2004).

4.5. Sensitivity analysis

We assessed the relative significance of the dimensionless independent parameters (H/d, α, θ, F_D) influencing the dependent parameters (d_{sm}, d_{sd}) in Eqs. (8) and (9) by varying the independent parameters around their mean values in the experiments. These mean values of H/d, α, θ, and F_D were 0.4, 25.26°, 41°, and 2.843, respectively.

For this analysis, the average values (x) of all input variables related to H/d, α, θ, and F_D corresponding to d_{sm}/d and d_{sd}/d, were utilized as recommended by Ahmad (2013). Sensitivity and error analyses were performed by varying the average value of each of the four input parameters by ±10% (defined as Δx), and observing the corresponding changes in the dependent variables (defined

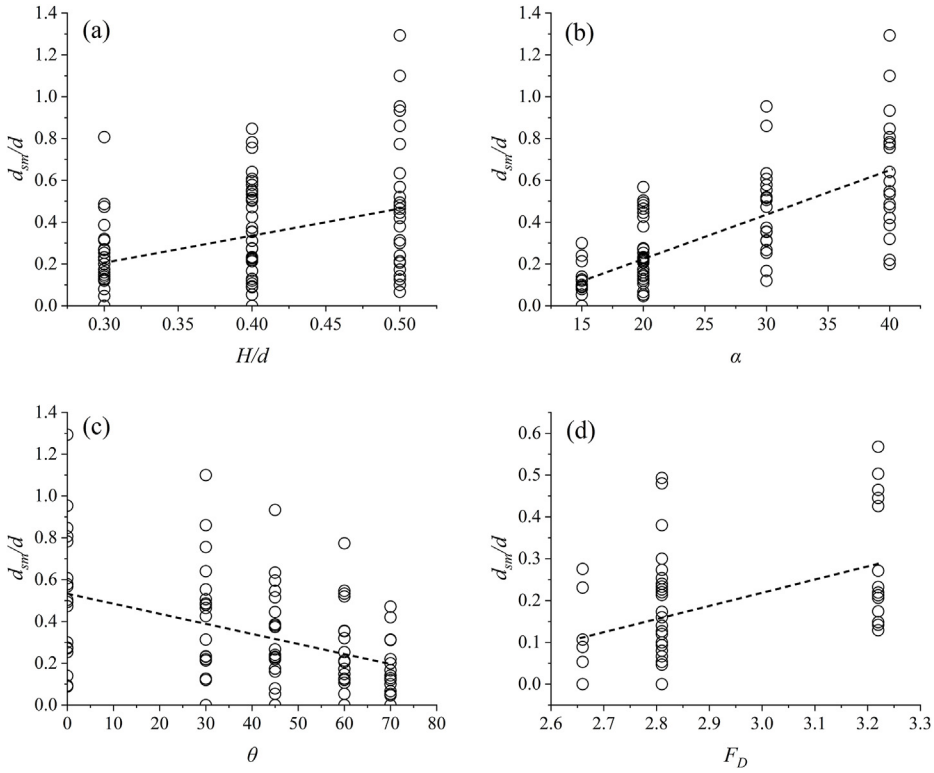

Fig. 15. Effect of various parameters on d_{sm}/d: (a) H/d, (b) α, (c) θ, and (d) F_D.

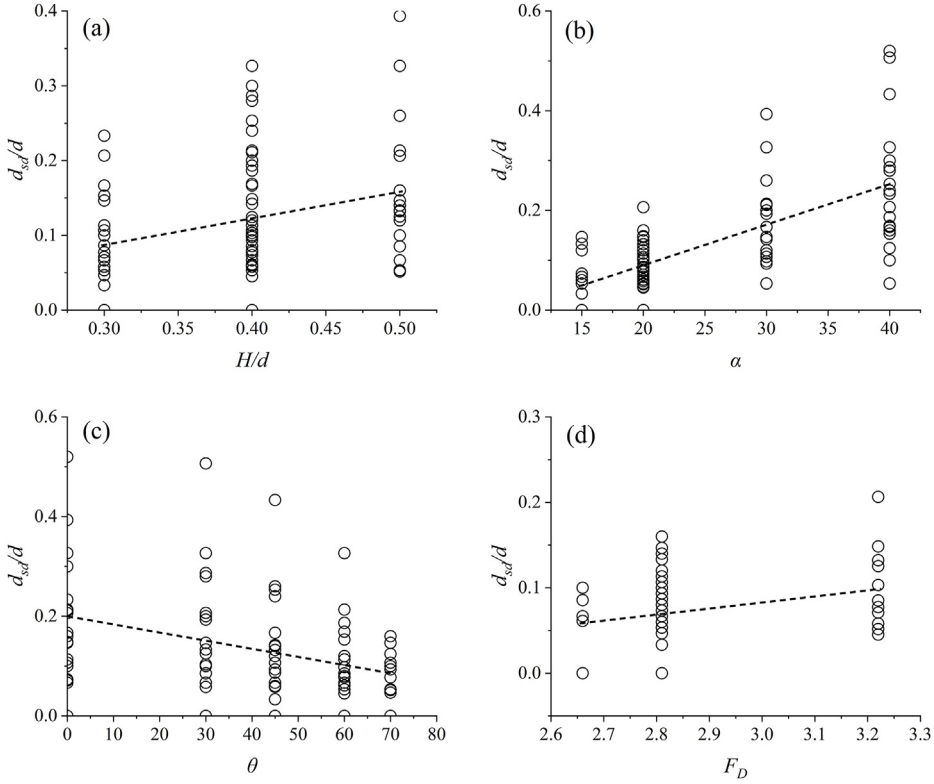

Fig. 16. Effect of various parameters on d_{sd}/d: (a) H/d, (b) α, (c) θ, and (d) F_D.

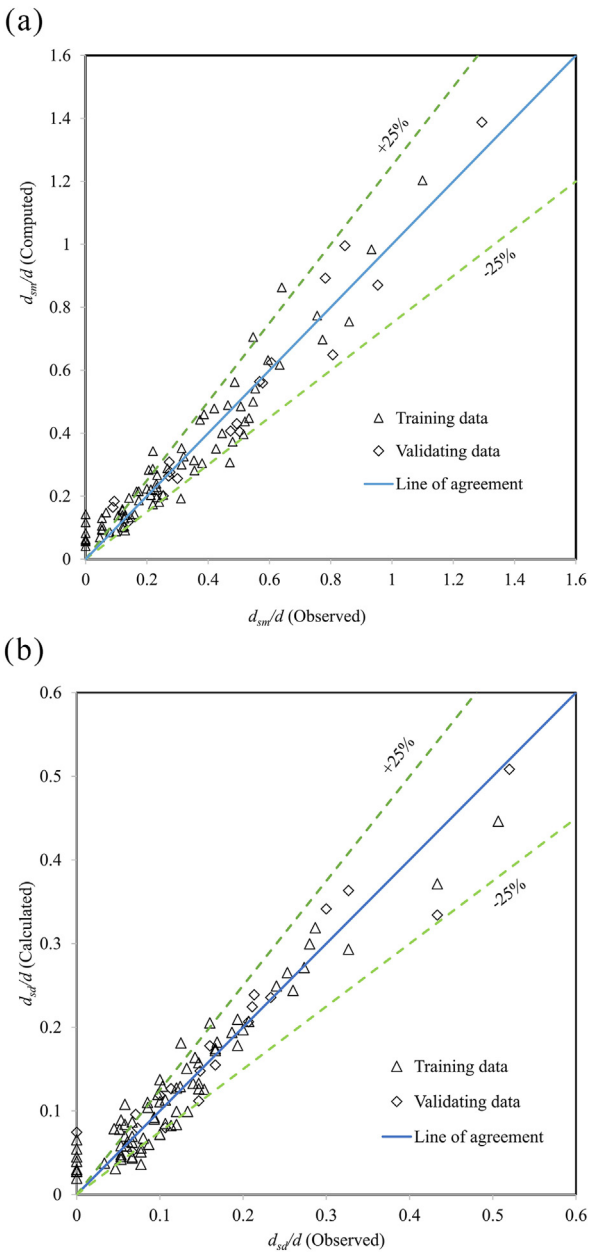

Fig. 17. Comparison of calculated (a) d_{sm}/d and (b) d_{sd}/d with observed values.

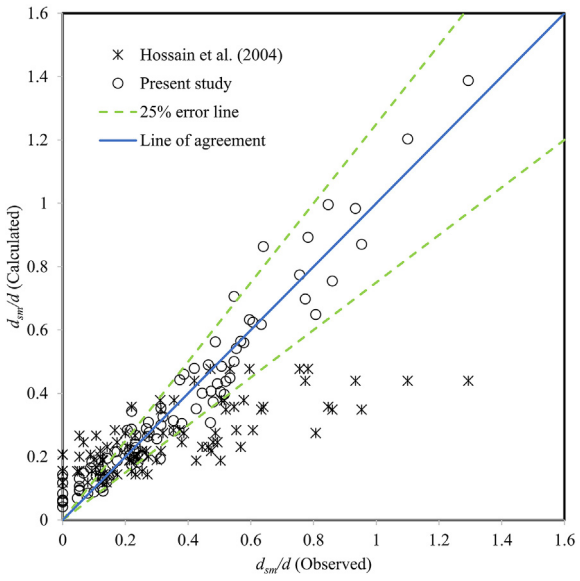

Fig. 18. Comparison between the equation of Hossain et al. (2004) and the proposed equation for maximum scour depth.

Table 3
Results of sensitivity analysis for d_{sm}/d.

	For 10% increment in x					For 10% decrement in x			
x	Δx	Δx	AS	RE	RS	Δy	AS	RE	RS
H/d	0.04	0.072	1.810	0.210	2.096	0.035	0.888	0.103	1.030
α	0.0441	0.082	1.855	0.237	2.37	0.044	0.996	0.127	1.273
θ	0.0716	−0.006	−0.085	−0.018	−0.178	−0.03	−0.419	−0.087	−0.87
F_D	0.284	0.093	0.327	0.270	2.698	0.052	0.182	0.150	1.499

Table 4
Results of sensitivity for d_{sd}/d.

	For 10% increment in x					For 10% increment in x			
x	Δx	Δy	AS	RE	RS	Δy	AS	RE	RS
H/d	0.04	0.0296	0.74	0.216	2.16	0.0154	0.386	0.1127	1.127
α	0.0441	0.0291	0.660	0.2125	2.125	0.0153	0.348	0.112	1.119
θ	0.0716	−0.0014	−0.02	−0.010	−0.1024	−0.009	−0.13	−0.066	−0.657
F_D	0.284	0.0217	0.076	0.158	1.583	0.010	0.035	0.073	0.730

as Δy). The error was evaluated using three indices known as absolute sensitivity (AS) = $\Delta y/\Delta x$, relative sensitivity (RS) = $(x \times \Delta y)/(y \times \Delta x)$, and relative error (RE) = $\Delta y/y$, where Δy represents the error in the output parameter, defined as the difference between the output values predicted for inputs x and $(x + \Delta x)$. The sensitivity analysis for d_{sm}/d is given in Table 3, revealing that d_{sm}/d which is the most sensitive to F_D followed by α and H/d. The relative sensitivity of F_D is about 1.26 times that of α and about 1.3 times that of H/d, for a 10% increment in x. However, for a 10% reduction in x, the relative sensitivity of F_D is about 1.18 times that of α and about 1.5 times that of H/d. The sensitivity analysis for d_{sd}/d is given in Table 4, showing that d_{sd}/d which is the most sensitive to H/d followed by α and F_D. The relative sensitivity of H/d is about 1.02 times that of α and about 1.36 times that of F_D, for a 10% increment in x. However, for a 10% reduction in x, the relative sensitivity of H/d is about 1.01 times that of α and about 1.54 times that of F_D. In both cases, θ is relatively less sensitive compared to other parameters.

5. Conclusions and recommendations

In river engineering, determining the maximum scour depth is critically important in the design of hydraulic structures as the local scour surrounding the structure impacts its structural stability. A series of experiments was performed in clear-water conditions on

various combinations of governing parameters with different flow regimes. It is found that the maximum scour hole occurs near the submerged vane and extends downstream of the vane. The maximum scour depth increases with increased H/d ratio, angle of attack, and densimetric Froude number. The rectangular shape generates a strong horseshoe vortex at the leading edge of the vane and dissipates quickly, producing a significant local scour on the pressure side of the vane. We observed that cutting the leading-edge w.r.t vertical axis or bevel shape of the submerged vane decreased the horseshoe vortex significantly, which reduced the local scour depth at the leading edge compared to the rectangular vane. The bevel shape of submerged vane is more effective in reducing local scour around the vane than reducing extended downstream scour. We propose empirical Eqs. (8) and (9) to calculate the maximum scour depth around the vane and the extended scour in the downstream channel based on the data collected in the current investigation. The calculated values of maximum scour depth around the vane and the extension of the scour downstream of the vane offer good correlation with the observed data. The densimetric Froude number of the flow and the angle of attack have the largest influence on the maximum depth of the local scour. At the same time, the height of the vane is the most sensitive parameter affecting the extension of the scour in the downstream channel. Although bevel angle exhibits relatively lower sensitivity compared to other parameters, it remains an effective method for reducing local scour around the vane. Furthermore, the bevel shape offers a cost-effective alternative, as it requires less material compared to the rectangular vane design. The present study is limited to a single size of cohesionless sediment and it specifically considers clear-water scour conditions, wherein no sediment is transported from the upstream region. In future studies taper, curved, and porous vanes could be used to find the most efficient shape to limit the local scour. A field study could be conducted to minimize scale effects and to validate the findings from the laboratory study.

Declaration of competing interest

The authors declare that they have no known competing financial interests or personal relationships that could have appeared to influence the work reported in this paper.

CRediT authorship contribution statement

Anirban Mandal: Writing – original draft, Software, Methodology, Investigation, Formal analysis, Data curation. **Zulfequar Ahmad:** Writing – review & editing, Validation, Supervision, Methodology, Investigation. **Erik Mosselman:** Writing – review & editing, Supervision, Methodology.

Data availability statement

The data supporting this investigation are accessible from the corresponding author upon reasonable request.

Permission to reproduce material from other sources

We do not use any material from external sources in our present study.

Funding

There were no funding sources for this research.

Acknowledgements

We extend our profound gratitude and heartfelt thanks to the Civil Engineering Department, IIT Roorkee, for offering a supportive environment and essential resources for conducting the research and analysis work. Special thanks to Dr. Mohd Faisal Ansari and Dr. Subhojit Kadia for their valuable discussions and feedback. Additionally, the authors express their gratitude to the anonymous peer reviewers for their valuable feedback, which has greatly enhanced the overall quality of the paper.

Notations

H	vane height (m)
L	vane length (m)
t	vane thickness (m)
A	angle of attack (°)
Θ	bevel angle (°)
Q	discharge (m^3/s)
V	average velocity (m/s)
d_{50}	sediment size (mm)
σ_g	geometric standard deviation
D	water depth (m)
B	channel width (m)
G	acceleration due to gravity (m/s^2)
P	mass density of flowing fluid (kg/m^3)
ρ_s	mass density of the sediment (kg/m^3)
M	dynamic viscosity of the flowing fluid ($(N\cdot s)/m^2$)
F_D	densimetric Froude number
N	kinematic viscosity (m^2/s)
d_s	maximum scour depth (m)
τ_c	critical shear stress (N/m^2)
u_*	approaching flow shear velocity (m/s)
u_{*_c}	critical shear velocity of the bed sediment (m/s)
R	hydraulic radius (m)
S	bed slope
u	streamwise velocity at a point (m/s)
v	lateral velocity at a point (m/s)
w	vertical velocity at a point (m/s)
X	streamwise distance along the length of the flume
Z	lateral distance across the width of the flume
Y	depth (or height) from initial bed level in the vertical direction
d_{sm}	maximum local scour depth around the vane (m)
d_{sd}	extension of the scour hole downstream of the vane (m)
d_s	scour depth at any point (m)

Appendix 1.1

Table 5
Scheme of experimentation

Run No.	Discharge, Q (m^3/s)	Angle of attack, α (°)	Vane height to depth ratio, H/d	Bevel angle, θ (°)	d_{sm}/d	d_{sd}/d
R1	0.082	15	0.3	0	0.140	0.067
R2	0.082	15	0.3	30	0.127	0.067
R3	0.082	15	0.3	45	0.080	0.033
R4	0.082	15	0.3	60	0.000	0.000
R5	0.082	15	0.3	70	0.000	0.000
R6	0.082	15	0.4	0	0.093	0.073
R7	0.082	15	0.4	30	0.120	0.067
R8	0.082	15	0.4	45	0.053	0.060
R9	0.082	15	0.4	60	0.053	0.053
R10	0.082	15	0.4	70	0.000	0.000
R11	0.082	15	0.5	0	0.300	0.147
R12	0.082	15	0.5	30	0.213	0.133
R13	0.082	15	0.5	45	0.240	0.120
R14	0.082	15	0.5	60	0.127	0.067
R15	0.082	15	0.5	70	0.100	0.053
R16	0.082	20	0.3	0	0.253	0.107
R17	0.082	20	0.3	30	0.220	0.100
R18	0.082	20	0.3	45	0.160	0.087
R19	0.082	20	0.3	60	0.120	0.067
R20	0.082	20	0.3	70	0.047	0.047
R21	0.082	20	0.4	0	0.273	0.113
R22	0.082	20	0.4	30	0.233	0.100
R23	0.082	20	0.4	45	0.227	0.093
R24	0.082	20	0.4	60	0.120	0.080
R25	0.082	20	0.4	70	0.053	0.053
R26	0.082	20	0.5	0	0.493	0.160
R27	0.082	20	0.5	30	0.480	0.147
R28	0.082	20	0.5	45	0.380	0.140
R29	0.082	20	0.5	60	0.173	0.120
R30	0.082	20	0.5	70	0.067	0.100
R31	0.082	30	0.3	0	0.473	0.167
R32	0.082	30	0.3	30	0.313	0.147
R33	0.082	30	0.3	45	0.267	0.107
R34	0.082	30	0.3	60	0.253	0.113
R35	0.082	30	0.3	70	0.120	0.053
R36	0.082	30	0.4	0	0.607	0.213
R37	0.082	30	0.4	30	0.553	0.193
R38	0.082	30	0.4	45	0.373	0.167
R39	0.082	30	0.4	60	0.353	0.120
R40	0.082	30	0.4	70	0.167	0.093
R41	0.082	30	0.5	0	0.953	0.393
R42	0.082	30	0.5	30	0.860	0.327
R43	0.082	30	0.5	45	0.633	0.260
R44	0.082	30	0.5	60	0.520	0.213
R45	0.082	30	0.5	70	0.313	0.147
R46	0.082	40	0.3	0	0.807	0.233
R47	0.082	40	0.3	30	0.487	0.207
R48	0.082	40	0.3	45	0.387	0.167
R49	0.082	40	0.3	60	0.320	0.153
R50	0.082	40	0.3	70	0.200	0.053
R51	0.082	40	0.4	0	0.847	0.327
R52	0.082	40	0.4	30	0.640	0.287
R53	0.082	40	0.4	45	0.547	0.253
R54	0.082	40	0.4	60	0.547	0.187
R55	0.082	40	0.4	70	0.220	0.100
R56	0.082	40	0.5	0	1.293	0.520
R57	0.082	40	0.5	30	1.100	0.507
R58	0.082	40	0.5	45	0.933	0.433
R59	0.082	40	0.5	60	0.773	0.327
R60	0.082	40	0.5	70	0.420	0.160
R61	0.058	15	0.4	0	0.089	0.000
R62	0.058	15	0.4	30	0.000	0.000
R63	0.058	15	0.4	45	0.000	0.000
R64	0.058	15	0.4	60	0.000	0.000
R65	0.058	15	0.4	70	0.000	0.000
R66	0.058	20	0.4	0	0.276	0.100
R67	0.058	20	0.4	30	0.231	0.086
R68	0.058	20	0.4	45	0.231	0.067
R69	0.058	20	0.4	60	0.107	0.061
R70	0.058	20	0.4	70	0.053	0.000

Table 5 (*continued*)

Run No.	Discharge, Q (m^3/s)	Angle of attack, α (°)	Vane height to depth ratio, H/d	Bevel angle, θ (°)	d_{sm}/d	d_{sd}/d
R71	0.058	30	0.4	0	0.578	0.211
R72	0.058	30	0.4	30	0.507	0.200
R73	0.058	30	0.4	45	0.516	0.142
R74	0.058	30	0.4	60	0.356	0.098
R75	0.058	30	0.4	70	0.311	0.107
R76	0.058	40	0.4	0	0.782	0.300
R77	0.058	40	0.4	30	0.756	0.280
R78	0.058	40	0.4	45	0.596	0.240
R79	0.058	40	0.4	60	0.533	0.169
R80	0.058	40	0.4	70	0.471	0.124
R81	0.092	20	0.3	0	0.271	0.071
R82	0.092	20	0.3	30	0.232	0.058
R83	0.092	20	0.3	45	0.174	0.058
R84	0.092	20	0.3	60	0.148	0.077
R85	0.092	20	0.3	70	0.129	0.077
R86	0.092	20	0.4	0	0.503	0.148
R87	0.092	20	0.4	30	0.426	0.103
R88	0.092	20	0.4	45	0.219	0.058
R89	0.092	20	0.4	60	0.213	0.045
R90	0.092	20	0.4	70	0.129	0.077
R91	0.092	20	0.5	0	0.568	0.206
R92	0.092	20	0.5	30	0.465	0.125
R93	0.092	20	0.5	45	0.445	0.132
R94	0.092	20	0.5	60	0.206	0.085
R95	0.092	20	0.5	70	0.142	0.052

References

Ahmad, Z. (2013). Prediction of longitudinal dispersion coefficient using laboratory and field data: Relationship comparisons. *Hydraulics Resources, 44*(2), 362–376.

Ansari, M. F., & Ahmad, Z. (2024). Scour pattern at zero-degree confluent channels. *Acta Geophysica, 72*, 3547–3561.

Azizipour, M., Meymani, F. A., & Shooshtari, M. M. (2020). Enhancing scour protection in river bends: A novel slotted bank-attached vane. *Water Science and Technology: Water Supply, 20*(6).

Baltazar, J., Alves, E., Bombar, G., & Cardoso, A. H. (2021). Effect of a submerged vane-field on the flow pattern of a movable bed channel with a 90^0 lateral diversion. *Water, 13*, 828.

Barani, G. A., & Sardo, M. S. (2013). Experimental investigation of submerged vanes shape effect on river-bend stability. *Hydraulic Structures, Spring, 1*(1), 35–41.

Barkdoll, B. D., Ettema, R., & Odgaard, A. J. (1999). Sediment control at lateral diversions: Limits and enhancements to vane use. *Journal of Hydraulic Engineering, ASCE, 125*(8), 862–870.

Bejestan, M. S., & Azizi, R. (2012). Experimental investigation of scour depth at the edge of different submerged vanes shapes. In *World environmental and water resources congress* (pp. 1376–1385). Reston, VA, USA: ASCE.

Best, J., & Ashworth, P. (1994). A high-resolution ultrasonic bed profiler for use in laboratory flumes. *Journal of Sedimentary Research, 64*(3).

Buckingham, E. (1915). *Model experiments and the forms of empirical equations, 37* pp. 263–292. Transactions of the American Society of Mechanical Engineers.

Dey, L., Barbhuiya, A. K., & Biswas, P. (2017). Experimental study on bank erosion and protection using submerged vane placed at an optimum angle in a 180^0 laboratory channel Bend. *Geomorphology, 283*, 32–40.

Fathi, A., & Zomorodian, S. M. (2018). Effect of submerged vanes on scour around a bridge abutment. *KSCE Journal of Civil Engineering, 22*(7), 2281–2289.

Goring, D. G., & Nikora, V. I. (2002). Despiking acoustic Doppler velocimeter data. *Journal of Hydraulic Engineering, 128*(1), 117–126.

Gumgum, F., & Cardoso, A. H. (2022). Optimizing the desilting efficiency of submerged vane fields at lateral diversions. *Journal of Hydraulic Engineering, ASCE, 149*(1), 04022031(1–12).

Gupta, U. P., Ojha, C. S. P., & Sharma, N. (2006). Vorticity with different shapes of submerged vanes. *ISH Journal of Hydraulic Engineering, 12*(1), 13–26.

Gupta, U. P., Sharma, N., & Ojha, C. S. P. (2007). Performance evaluation of tapered vane. *Journal of Hydraulic Research, 45*(4), 472–477.

Hamidi, M., Sadeqlu, M., & Khalili, A. M. (2024). Investigating the design and arrangement of dual submerged vanes as mitigation countermeasure of bridge pier scour depth using a numerical approach. *Ocean Engineering, 299*, 117270.

Hossain, M. M., Islam, M. R., Saha, S., Ferdousi, S., Van Zwol, B., Zijlstra, R., & Mosselman, E. (2004). Laboratory tests on scour around bottom vanes. In *Proceedings 2nd international Conference on Scour and erosion, (ICSE-2). November 14.-17., 2004, Singapore*.

Klovsky, A. V., & Kozlov, D. V. (2019). Generation of artificial transverse circulation in an open channel flow by submerged vanes. *Journal on Construction and Architecture, 14*(9), 1158–1166.

Mandal, A., & Ahmad, Z. (2024). Experimental study on local scour around submerged vanes of different bevel angles. In *10th international symposium on hydraulic structures, ISSN 0374-0056, Zurich, Switzerland*.

Mandal, A., Gautam, H., & Ahmad, Z. (2024). Sediment control and flow redistribution with submerged vanes: A review. *Water Practice and Technology, 19*(5), 2197.

Marelius, F., & Sinha, S. K. (1998). Experimental investigation of flow past submerged vanes. *Journal of Hydraulic Engineering, ASCE, 124*(5), 542–545, https://doi.org/10.1061/(ASCE)0733-9429(1998)124:5(542)

Marsh, N. A., Western, A. W., & Grayson, R. B. (2004). Comparison of methods for predicting incipient motion for sand beds. *Journal of Hydraulic Engineering, 130*(7), 616–621.

Nikora, V. I., Goring, D. G., & Biggs, B. J. F. (1998). Silverstream eco-hydraulics flume: Hydraulic design and tests. *Journal of Marine and Freshwater Research, 32*(4), 607–620.

Odgaard, A. J. (2009). *River training and sediment management with submerged vanes*. USA: American Society of Civil Engineers.

Odgaard, A. J., & Kennedy, J. F. (1983). River-bend bank protection by submerged vanes. *Journal of Hydraulic Engineering, ASCE, 109*(8), 161–173.

Odgaard, A. J., & Mosconi, C. E. (1987). Streambank protection by submerged vanes. *Journal of Hydraulic Engineering, ASCE, 113*(4), 520–536.

Odgaard, A. J., & Spoljaric, A. (1986). Sediment control by submerged vanes. *Journal of Hydraulic Engineering, ASCE, 112*(12), 1164–1181.

Odgaard, A. J., & Spoljaric, A. (1989). Sediment control by submerged vanes. Design basis. *River Meandering, 12*, 127–151.

Odgaard, A. J., & Wang, Y. (1991a). Sediment management with submerged vanes. I: Theory. *Journal of Hydraulic Research, 117*(3), 267.

Ouyang, H. T. (2009). Investigation on the dimensions and shape of a submerged vane for sediment management in alluvial channels. *Journal of Hydraulic Engineering, ASCE, 135*(3), 209–217.

Ouyang, H. T., & Lin, C. P. (2016). Characteristics of interactions among a row of submerged vanes in various shapes. *Journal of Hydro-environment Research, 13*, 14–25.

Rajaratnam, N. (1981). Erosion by plane turbulent jets. *Journal of Hydraulic Research, 19*(4), 339–358.

Sarlak, H., Bejestan, M. S., & Sajjadi, S. M. (2023). Experimental investigation of the effect of permeability and angle of gabion submerged vane on bed topography. *Arabian Journal of Geosciences, 16*, 288.

Tasar, B., Unes, F., Gemici, E., & Zelenakova, M. (2023). Experimental and numerical study on flow control using 3-array submerged vane in laboratory channel bend. *Water, 15*, 659.

Teronpi, J., & Misra, U. K. (2015). Experimental investigation of local scour around submerged vanes. *International Journal of Innovative Research in Advanced Engineering, 2*(7), 21–24.

Vaghefi, M., Zarei, E., Ahmadi, G., & Behroozi, A. M. (2023). Experimental analysis of submerged vanes' configuration for mitigating local scour at piers in a sharp bend: Influence of quantity, length, and orientation. *Ocean Engineering, 289*(1), 116267.

Wang, Y., & Odgaard, A. J. (1993). Flow control with vorticity. *Journal of Hydraulic Research, IAHR, 31*(4), 549–562.

Yarahmadi, M. B., & Bejestan, M. S. (2016). Sediment management and flow patterns at river bend due to triangular vanes attached to the bank. *Journal of Hydro-environment Research, 10*, 64–75.